

# Breakthrough modeling and experimental design for *o*-xylene dynamic adsorption onto clay material

Nadim Fakhfakh<sup>1,2</sup> · Nesrine Dammak<sup>1,2</sup> · Mourad Benzina<sup>1,2</sup>

Received: 27 December 2016 / Accepted: 29 May 2017 / Published online: 17 June 2017  
© Springer-Verlag Berlin Heidelberg 2017

**Abstract** The adsorption of *o*-xylene onto raw clay material in a fixed bed using a thermal conductivity detector gas chromatography was investigated. Experimental and theoretical studies were established to evaluate the removal efficiency of *o*-xylene by adsorption on clay materials and to predict kinetic parameters. Column data were describing at different conditions using Bohart–Adams, Wolborska, Thomas, Yoon and Nelson, dose–response, and bed depth service time models. All used models were satisfactory to predict the breakthrough curves. A suitable advection–dispersion–sorption (ADS) model has been also developed to simulate the measured data, based on the nature of the various equilibrium relationships of solid–gas and diverse descriptions of the mass transfer processes within of the adsorbent particle. The experiments can be fitted with high correlated coefficient  $R^2 = 0.996$ .

**Keywords** Modeling · Breakthrough · Dynamic adsorption · Diffusion

---

Responsible editor: Marcus Schulz

Nadim Fakhfakh and Nesrine Dammak contributed equally to this work.

✉ Nadim Fakhfakh  
fakhfakhnadim@yahoo.fr

<sup>1</sup> University of Sfax, 3029 Sfax, Tunisia

<sup>2</sup> Water, Energy and Environment Laboratory, ENIS B.P. W, 3038 Sfax, Tunisia

## Nomenclature

$a$	Dose–response constant
$a_p$	Specific and volumetric surface for spherical particle ( $\text{m}^{-1}$ )
$C_0$	Inlet <i>o</i> -xylene concentration ( $\text{g m}^{-3}$ )
$C$	Outlet concentration of the solute in the fluid phase at time $t$ ( $\text{g m}^{-3}$ )
$C_i$	Concentration of solute in the solid–gas interface ( $\text{g m}^{-3}$ )
$D_{\text{eff}}$	Effective coefficient diffusion ( $\text{m}^2 \text{min}^{-1}$ )
$D_{\text{ax}}$	The axial dispersion coefficient ( $\text{m}^2 \text{min}^{-1}$ )
$d_p$	Particle diameter (m)
$K_{\text{BA}}$	Kinetic constant of Bohat–Adams model ( $\text{m}^3 \text{g}^{-1} \text{min}^{-1}$ )
$K_{\text{BDST}}$	Kinetic constant of BDST model ( $\text{m}^3 \text{g}^{-1} \text{min}^{-1}$ )
$K_{\text{C}}$	Kinetic constant of Clark ( $\text{m}^3 \text{g}^{-1} \text{min}^{-1}$ )
$k_f$	Mass transfer coefficient in the fluid phase ( $\text{m s}^{-1}$ )
$K_{\text{L}}$	Langmuir constant
$k_s$	Mass transfer coefficient in solid phase ( $\text{m s}^{-1}$ )
$K_{\text{YN}}$	Kinetic constant of Yoon–Nelson model ( $\text{min}^{-1}$ )
$K_{\text{Th}}$	Kinetic constant of Thomas model ( $\text{m}^3 \text{g}^{-1} \text{min}^{-1}$ )
$L_c$	Column length (mm)
$m$	Amount of adsorbent in the column (g)
$n$	Freundlich constant
$N_0$	Maximum volumetric sorption capacity of bed ( $\text{g m}^{-3}$ )
$Q$	Flow rate ( $\text{m}^3 \text{min}^{-1}$ )
$q_0$	Maximum adsorption capacity ( $\text{mg g}^{-1}$ )
$q$	Average weight of the solute adsorbed at time $t$ , per kg of fresh adsorbent ( $\text{mg g}^{-1}$ )
$q_i$	The weight of the solute adsorbed at time $t$ , per kg of fresh adsorbent solid–gas interface ( $\text{mg g}^{-1}$ )
$S$	Cross section of the column ( $\text{m}^2$ )

$t$	Time (min)
$u$	Linear velocity ( $\text{m min}^{-1}$ )
$v$	Interstitial fluid velocity ( $\text{m min}^{-1}$ ); ( $v = \frac{u}{\varepsilon}$ )
$Z$	Bed height (m)
$\beta_a$	The kinetic coefficient of the external mass transfer ( $\text{min}^{-1}$ )
$\rho$	Density of the bed ( $\text{g m}^{-3}$ )
$\varepsilon$	Void fraction of the bed

## Introduction

Volatile organic compounds (VOCs) which have some toxicity have been contributing in some scale to atmospheric pollution (Pires et al. 2001). Therefore and due to the increasing attention on the environmental protection, there is growing public concern about the widespread contamination of air in order to reduce the emissions (Lin and Cheng 2002; Dammak et al. 2015).

Therefore, industries require cheap and effective technologies to reduce the concentration of these gases and vapor to accepted levels. Adsorption which is becoming a more and more popular technique for removal of pollutants has been found to be effective at low concentration (Gupta and Verma 2002). Among VOC, *o*-xylene is generally considered to be one of the organic pollutants discharged into the environment causing toxic effects on humans (Jones 1999).

The effectiveness of a clay adsorbent can be evaluated from the S-shaped breakthrough curves (Chu 2004; Muhamad et al. 2010; Dammak et al. 2013).

The aim of the present work is to investigate the effects of flow rate, bed depth, and the *o*-xylene inlet concentration on adsorption capacity by a fixed-bed column. In general, the models proposed for the recovery of gaseous pollutants assume that the adsorption mechanism is governed by mass transfer monitoring followed by the adsorption equilibrium and the kinetics of adsorption (Malek and Farooq 1997). In order to visualize the relationship between the various parameters influencing the mass transfer and the adsorption in the adsorbent bed of clay material, Bohart–Adams, Wolborska, Thomas, Yoon–Nelson, Clark, dose–response, bed depth service time (BDST), and mass transfer models were used to fit the experimental adsorption results. The results of coefficients obtained with modeling the continuous process can be scaled to an actual industrial column.

## Materials and methods

### Adsorbate and adsorbent

Clay material with average particle diameter of 0.85 mm was supplied from Jebel Sbih located in south of Tunisia in the region of Skhira. *O*-xylene ( $\text{C}_8\text{H}_{10}$ , 98%) was purchased from

Fluka Analytical. The chemical composition of adsorbent was determined by X-ray fluorescence with an ARL1 9800 XP spectrometer. The mineralogical composition was determined by a Rigakud-Max 2200 model X-ray diffractometer. The specific area was determined by ASAP 2010 V5.02 H Unit 1 Serial # 844 apparatus.

### Adsorption in continuous fixed-bed column

The column adsorption tests were applied in stainless steel column of 0.4-m height and 0.01-m inner diameter. Clay material was packed into the column. A certain amount of clay material (0.1, 0.15, 0.2 m) was loaded into the column. All the experiments were carried out at 20 °C using mixed gas of *o*-xylene and nitrogen as a gas carrier. The saturated vapor pressure of *o*-xylene was used to produce the desired concentrations by diluting with pure nitrogen gas in a flow of  $0.27\text{--}0.63 \times 10^{-3} \text{ m}^3 \text{ min}^{-1}$  to obtain *o*-xylene inlet concentration ( $C_0$ ) of  $6.4\text{--}11.11 \text{ g m}^{-3}$ . Comparable operator conditions are used in similar researches (Lee et al. 1990; Minceva and Rodrigues 2004; Chafik et al. 2009; Huang et al. 2009).

The outlet concentrations were monitored using a gas chromatography (Shimadzu GC-2014) equipped with a thermal conductivity detector (TCD) and a packed column using a  $\text{N}_2$  carried gas. The adsorption data were taken at 3-min sampling interval to monitor the adsorbent breakthrough until the adsorbent was saturated.

Then, the breakthrough curves with the form of variations of  $C/C_0$  versus time were obtained. Figure 1 illustrates the experimental configuration used for adsorption of *o*-xylene on a fixed bed.

### Experimental design

A nonlinear model of degree 2 is sufficient to translate the relation cause and effect between the density ( $X_1$ ), Langmuir constant ( $X_2$ ), and the axial dispersion ( $X_3$ ) on one hand and

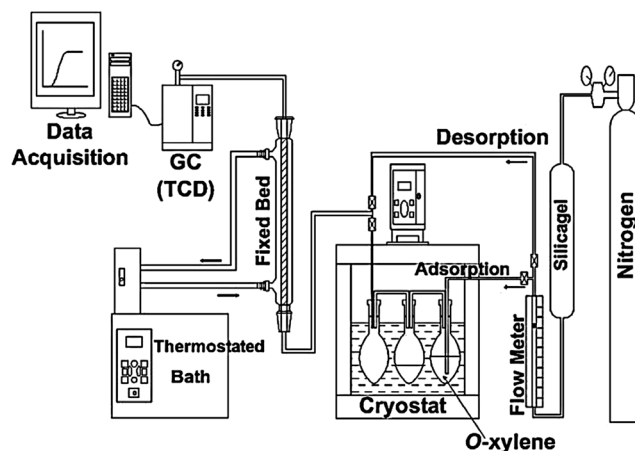


Fig. 1 Experimental apparatus of *o*-xylene vapor sorption

the breakthrough time as studied answer ( $\hat{Y}$ ) on the other hand. The calculation was performed with the statistical software “New Methodology for Efficient Research using Optimal Design (NEMROD)” to estimate the response in the predefined area.

$$Y = b_0 + \sum_{i=1}^3 b_i X_i + \sum_{i=1}^3 b_{ii} X_i^2 + \sum_{i < j}^3 b_{ij} X_i X_j \tag{1}$$

where  $\hat{Y}$  is the predicted response for breakthrough time,  $b_0$  the offset term,  $b_i$  the linear effect,  $b_{ii}$  the squared effect, and  $b_{ij}$  is the interaction effect.

The test factors were coded according to the following equation:

$$X_i = \frac{Z_i - Z_0}{\Delta Z} \tag{2}$$

where  $Z_i$  is the value of the independent variables,  $Z_0$  is the natural value of the independent variables at the center point, and  $\Delta Z$  is the step change value.

## Results and discussions

### Clay characterization

The clay material composition is presented in Table 1. SiO<sub>2</sub> and Al<sub>2</sub>O<sub>3</sub> are the major constituents of the clay with trace amounts of other oxides. The percentage of iron is relatively high which is typical of Tunisian clays. The mineralogical study by X-ray diffraction of clay material adsorbent presented in Fig. 2 shows that this material is mainly composed of 67% of the smectite (S), 9% of kaolinite (K), and a percentage of 11 and 13% of quartz (Q) and calcite (C), respectively. The specific surface area of clay adsorbent was 67 m<sup>2</sup> g<sup>-1</sup>. More details of clay characterization are presented in previous paper (Dammak et al. 2015).

### Dynamic adsorption

The effect of bed depth on the *o*-xylene adsorption in continuous packed bed was examined by varying the bed depth from 0.1 to 0.2 m where the inlet concentration and flow rate were constant at 6.4 g m<sup>-3</sup> and 0.63 × 10<sup>-3</sup> m<sup>3</sup> min<sup>-1</sup>, respectively.

Figure 3 shows that the breakthrough time increased with the increase of bed depth. An increase in the bed height rises the distance for the mass transfer zone to reach the end of column and therefore an increase in the breakthrough time. *O*-xylene adsorption capacity increased (Table 2) when bed depth decreases as well as the breakthrough curve becomes steeper due to the increase of the mass transfer coefficient. The adsorption along the bed height is highest at the front face of column and decreases gradually in the bed exit. For adsorbents loaded as a random packing in column, a particle can be obstructed by another one in front of it. Thus, exposure time between particle and adsorbate molecules is reduced as well as adsorbed amount (Lua and Jandia 2009; Leyva-Ramos et al. 2007).

Experiments were also led at different inlet *o*-xylene concentrations to observe the continuous adsorption performance of clay material. The breakthrough curves resulted by varying inlet *o*-xylene concentration from 6.4 to 11.11 g m<sup>-3</sup> at 0.63 × 10<sup>-3</sup> m<sup>3</sup> min<sup>-1</sup> flow rate and 0.1-m bed height are shown in Fig. 3. With high inlet *o*-xylene concentrations, adsorbent is more quickly saturated and breakthrough curves were delayed. Taking the column adsorption performance into account, lowest inlet *o*-xylene concentration leads to better *o*-xylene removal (Table 2).

Figure 3 shows the breakthrough curves obtained at different flow rates (0.63–11.11 × 10<sup>-3</sup> m<sup>3</sup> min<sup>-1</sup>), while bed height and inlet *o*-xylene concentration were held constant at 0.1 m and 6.4 g m<sup>-3</sup>, respectively. When the flow rate was reduced, breakthrough time increased and retained *o*-xylene decreased. This could be due to insufficient residence time of gas molecules in column in the case of high flow rate. At low flow rates, the thickness of the mass transfer boundary layer around the clay will raise, leading to enhanced external mass transfer resistance. These results are similar to those obtained by other researchers in fixed-bed adsorption studies for different VOC and different adsorbent materials (Huang et al. 2003; Yaneva et al. 2008; Zhang et al. 2010).

### Models for the initial part of breakthrough curve

A satisfactory design of a column adsorption process demands prediction of the breakthrough curve for effluents (Han et al. 2009). Over the years, several simple mathematical models have been developed for describing and analyzing the practical size column studies for the purpose of industrial applications (Kumar and Chakraborty 2009; Vinodhini and Das 2010).

**Table 1** Chemical composition of clay material

Compound	SiO <sub>2</sub>	Al <sub>2</sub> O <sub>3</sub>	CaO	Fe <sub>2</sub> O <sub>3</sub>	MgO	Cl	TiO <sub>2</sub>	Na <sub>2</sub> O	K <sub>2</sub> O	SO <sub>3</sub>	LSF
Percentage (%)	46.79	18.10	10.62	10.99	3.11	3.17	1.71	0.86	0.77	0.24	3.20

LSF low smoke fume

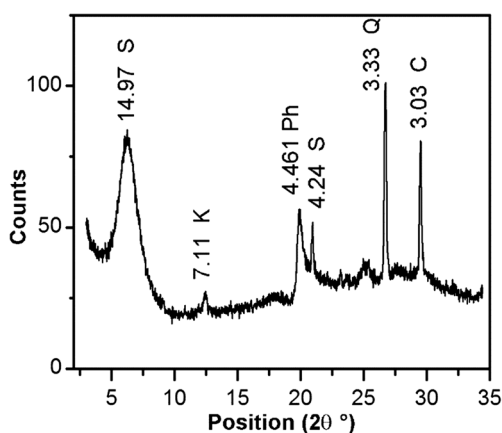


**Fig. 2** X-ray diffraction patterns of clay material (S smectite, K kaolinite, Ph phyllosilicate, Q quartz, C calcite)

Several models were developed to predict the breakthrough performance and to determine the adsorption capacity and kinetic constants of fixed-bed columns (Hasan et al. 2010; Rao et al. 2011).

#### Bohart–Adams model

In 1920, Bohart and Adams (Bohart and Adams 1920) derived an equation to describe vapor profiles in adsorbent filter beds, by reporting experimental data for chlorine transmission through charcoal filters. They showed qualitative agreement with the experimental vapor profiles. Many workers (Aksu and Gönen 2006; Hamdaoui 2006; Calero et al. 2009; Vijayaraghavan and Prabu 2006) have subsequently extended the model to describe and quantify other types of systems. This model does not take into account the external film resistance

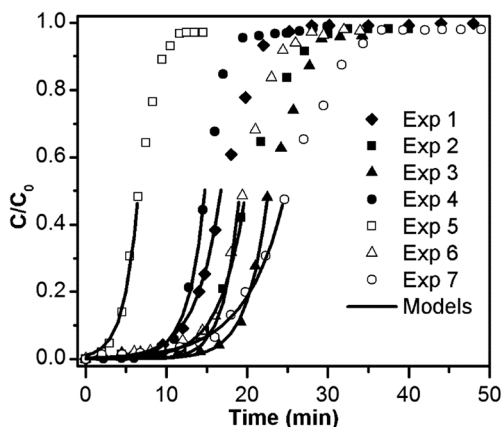


**Fig. 3** Experimental and initial part of breakthrough model curves for *o*-xylene onto clay material at different flow rates, bed heights, and inlet *o*-xylene concentrations.  $0.63 \times 10^{-3} \text{ m}^3 \text{ min}^{-1}$ , 0.1 m,  $6.4 \text{ g m}^{-3}$  (diamonds);  $0.63 \times 10^{-3} \text{ m}^3 \text{ min}^{-1}$ , 0.15 m,  $6.4 \text{ g m}^{-3}$  (filled squares);  $0.63 \times 10^{-3} \text{ m}^3 \text{ min}^{-1}$ , 0.2 m,  $6.4 \text{ g m}^{-3}$  (filled triangles);  $0.63 \times 10^{-3} \text{ m}^3 \text{ min}^{-1}$ , 0.1 m,  $8.77 \text{ g m}^{-3}$  (filled circles);  $0.63 \times 10^{-3} \text{ m}^3 \text{ min}^{-1}$ , 0.1 m,  $11.11 \text{ g m}^{-3}$  (empty squares);  $0.45 \times 10^{-3} \text{ m}^3 \text{ min}^{-1}$ , 0.1 m,  $6.4 \text{ g m}^{-3}$  (empty triangles);  $0.27 \times 10^{-3} \text{ m}^3 \text{ min}^{-1}$ , 0.1 m,  $6.4 \text{ g m}^{-3}$  (empty circles)

and the intraparticle mass transfer resistance and assumes that the adsorption is done directly on the adsorbent surface (Ko et al. 2000). The original equation was given in the form:

$$\frac{C}{C_0} = \frac{\exp(\tau)}{\exp(\tau) + \exp(\xi) - 1} \text{ with } \begin{cases} \tau = K_{BA} \times C_0 \times \left(t - \frac{Z}{v}\right) \\ \xi = \frac{K_{BA} \times N_0 \times Z}{v} \left(\frac{1-\varepsilon}{\varepsilon}\right) \end{cases} \quad (3)$$

where  $\tau$  and  $\xi$  are dimensionless time and distance coefficient, respectively,  $C_0$  is the initial *o*-xylene concentration,  $C$  is the concentration at time  $t$ ,  $K_{BA}$  is the kinetic constant of Bohart–Adams model,  $N_0$  is the maximum volumetric adsorption capacity of bed,  $Z$  is the bed depth,  $v$  is the *o*-xylene velocity and  $\varepsilon$  is the void fraction of the bed.

To apply the Bohart–Adams model in order to design adsorbent beds requires precise knowledge of  $K_{BA}$  and  $N_0$  parameters. To predict these parameters' effects of mass transfer, kinetics and equilibrium of adsorption should be determined. This fact is not easy, and Eq. (3) was fitted to the breakthrough data to determine these two parameters.

Bohart–Adams model is going to be applied to describe the primary part of the breakthrough curve, with concentration values lower than  $0.15C_0$  (Sarin et al. 2006).

To facilitate Eq. (3), it can be written as

$$\frac{C_0}{C} - 1 = \exp(\xi - \tau) - \exp(-\tau) \quad (4)$$

The term  $\exp(\tau)$  is usually small and can be neglected. For long times, the term  $Z/v$  can be also neglected. Insert logarithms in Eq. (4):

$$\ln\left(\frac{C_0}{C} - 1\right) = \frac{K_{BA} \times N_0 \times Z}{v} \left(\frac{1-\varepsilon}{\varepsilon}\right) - K_{BA} \times C_0 \times t \quad (5)$$

To predict the value of  $K_{BA}$  and  $N_0$  from early breakthrough points using plots of  $C/C_0$  against  $t$  at a given inlet concentration, bed depth and flow rate are likely using the nonlinear regression.

#### Wolborska model

Wolborska model (1989) is used to describe the dynamic adsorption for low concentrations breakthrough using mass transfer equations. It is given by the following equation:

$$\frac{C}{C_0} = \exp\left(\frac{\beta_a \times C_0 \times t}{N_0} - \frac{\beta_a \times Z}{u}\right) \quad (6)$$

where  $\beta_a$  the kinetic coefficient of the external mass transfer and  $N_0$  the maximum volumetric adsorption capacity of bed.

**Table 2** Column data and parameters obtained at diverse flow rates, bed heights, and inlet *o*-xylene concentrations

Exp. no.	Flow rate × 10 <sup>3</sup> (m <sup>3</sup> min <sup>-1</sup> )	Bed height (m)	Inlet concentration (g m <sup>-3</sup> )	Max adsorbed quantity (mg g <sup>-1</sup> )	Breakthrough time (min)	Saturation time (min)
1 (◆)	0.63	0.10	6.4	6.869	8.84	26.24
2 (■)	0.63	0.15	6.4	5.347	11.81	32.30
3 (▲)	0.63	0.20	6.4	4.581	15.17	36.98
4 (●)	0.63	0.10	8.77	6.231	8.95	27.80
5 (□)	0.63	0.10	11.11	4.734	3.87	15.16
6 (△)	0.45	0.10	6.4	5.633	9.95	32.46
7 (○)	0.27	0.10	6.4	4.360	10.00	44.16

The expression of the Wolborska solution is equivalent to the Bohart–Adams relation if the coefficient  $k_{BA}$  is equal to  $\beta_a/N_0$  (Guibal et al. 1995).

When Bohart–Adams and Wolborska models were fitted to the full part of the breakthrough curves, they showed low fitness for all the breakthrough curves (not shown). That is why these models were applied only for the initial part of the curves ( $C/C_0 < 0.5$ ) (Fig. 3).

Parameters of these models are summarized in Table 3. The saturation concentration  $N_0$  decreased with increasing bed depth. Kinetic constants  $k_{BA}$  and  $\beta_a$  are generally not affected by the variation of bed depth, inlet *o*-xylene concentration, or flow rate.

**Models for the total breakthrough curve**

*Thomas model*

Thomas model (1944) is the most used model for describing breakthrough curves in the case of a fixed-bed adsorption. This model assumes that the axial dispersion is negligible in

the column and the adsorption kinetics follows the Langmuir model (Morales Futulan et al. 2011). It is given by the following relation:

$$\frac{C}{C_0} = \frac{1}{1 + \exp\left[\left(\frac{K_{Th}}{Q}\right)(q_0 \times m - C_0 \times Q \times t)\right]} \tag{7}$$

where  $K_{Th}$  is the Thomas rate constant,  $q_0$  is the maximum concentration of the *o*-xylene in the solid phase,  $m$  is amount of adsorbent in the column, and  $Q$  is the flow rate of *o*-xylene.

*Yoon–Nelson model*

The Yoon–Nelson model (1984) is a relatively simple model developed for the first time to the adsorption of gases on activated charcoal. This model assumes that the rate of diminution in adsorption for every adsorbate molecule is relative to the probability of solute breakthrough on the adsorbent (Calero de Hoces et al. 2010). The equation for this model is

**Table 3** Bohart–Adams and Wolborska model parameters

Model parameters	Unity	Exp. no.						
		1	2	3	4	5	6	7
<b>Bohart–Adams</b>								
$K_{BA}$	m <sup>3</sup> g <sup>-1</sup> min <sup>-1</sup>	0.071	0.069	0.090	0.057	0.056	0.076	0.042
$N_0$	g m <sup>-3</sup>	5831	4566	3873	7506	4449	4783	3680
$R^2$	–	0.999	0.999	0.996	0.997	0.995	0.995	0.998
<b>Wolborska</b>								
$\beta_a$	min <sup>-1</sup>	511	390	396	633	370	424	198
$N_0$	g m <sup>-3</sup>	9660	7516	6258	11,430	6865	7894	6214
$R^2$	–	0.994	0.994	0.994	0.994	0.994	0.994	0.997

$$\frac{C}{C_0} = \frac{1}{1 + \exp(K_{YN}(t_{50}-t))} \quad (8)$$

where  $K_{YN}$  is the Yoon–Nelson constant and  $t_{50}$  is the time required for retaining 50% of the initial adsorbate.

#### Clark model

A simulation was described by Clark (1987) for breakthrough curves. The model defined was based on mass transfer theory and the nonlinear equation of Freundlich (Hamdaoui 2006):

$$\frac{C}{C_0} = \left( \frac{1}{1 + A \times e^{-r \times t}} \right)^{1/(n-1)} \quad \text{with} \quad \begin{cases} A = \exp\left(\frac{K_C \times N_0 \times Z}{u}\right) \\ r = K_C \times C_0 \end{cases} \quad (9)$$

$K_C$  is Clark constant and  $n$  is Freundlich constant.

Values of  $A$  and  $r$  can be determined via plot of  $C/C_0$  versus  $t$  at a given bed height and flow rate involving nonlinear regressive resolution.

#### Dose–response model

The dose–response model has been frequently used to describe different types of processes in biology such as biosorption in columns (Calero et al. 2009; Aksu and Gönen 2006; Yan et al. 2001). The dose–response model is represented by the equation

$$\frac{C}{C_0} = 1 - \frac{1}{1 + \left(\frac{C_0 \times Q \times t}{q_0 \times m}\right)^a} \quad (10)$$

where  $a$  is a constant.

#### Bed depth service time model

It is one of the most widely used models that describe heavy metal adsorption using a fixed-bed column. BDST is a simple model to estimate the relation between the breakthrough time and bed height according to different sorption parameters as inlet concentration of process. In this model, the adsorption capacity of the bed is founded on experimental measuring at different breakthrough times. This model does not take into account the external film resistance and the intraparticle mass transfer resistance, and the solute is adsorbed onto the adsorbent surface (Qaiser et al. 2009). The BDST model can be used to estimate the required bed depth for a given service time. It is given by equation

$$\frac{C}{C_0} = \frac{1}{1 + \exp\left[K_{BDST} \times C_0 \left(\frac{N_0}{C_0 \times u} Z - t\right)\right]} \quad (11)$$

where  $K_{BDST}$  is the adsorption rate constant that describes the mass transfer from fluid to the solid phase.

Table 4 lists the calculated Thomas, Yoon–Nelson, Clark, dose–response, and BDST model parameters from the experimental column data when inlet concentration, bed depth, and flow rate were varied. These parameters correspond to the best results of adsorption capacity obtained at a flow rate of  $0.63 \times 10^{-3} \text{ m}^3 \text{ min}^{-1}$ , inlet concentration of  $6.4 \text{ g m}^{-3}$ , and a bed depth of 0.1 m.

The Thomas, Yoon–Nelson, Clark, dose–response, and BDST models were modeled using Oakdale Engineering Data Fit 8.1 software.

The correlation coefficient values ranged from 0.994 to 0.999, indicating that all models were suitable for the description of the adsorption mechanisms for the total breakthrough curves (Table 4). Figure 4 shows the predicted and experimental breakthrough curves at different conditions and validates the correlation coefficient cited.

For Thomas and dose–response, the predicted maximum adsorption capacities ( $q_0$ ) were in agreement and did not show a larger deviation (1.54%) using these two models.

Adsorption capacity increases with the decrease of initial concentration, which may be attributed to a slower saturation of adsorbent in fixed bed at low inlet concentration. A low inlet concentration causes slow transport of *o*-xylene from the film layer to the surface of adsorbent. This implies a decreased diffusion coefficient and decreased mass transfer driving force (Tor et al. 2009).

Thomas and dose–response models are suitable for adsorption processes (Calero et al. 2009; Han et al. 2008). The constant  $K_{Th}$  that characterized the ratio of adsorbate transfer from the fluid to the solid phase increased with flow rate. Thus, at higher flow rate, adsorbates did not have enough time to diffuse into the adsorbent material, and they passed the column fast before equilibrium occurred. High flow rates will moderate the thickness of the mass transfer boundary layer around the clay, leading to reduce external mass transfer resistance. Similar observation was shown in similar research (Chen et al. 2011; Lua and Jandia 2009; Acheampong et al. 2013).

The Yoon–Nelson model adequately describes the experimental data. The constant  $k_{YN}$  of Yoon–Nelson model increased with increasing initial concentration. The time necessary to reach 50% of the retention,  $t_{50}$ , decreases significantly when the inlet concentration increased. The highest inlet concentration saturated the adsorption column more rapidly (Calero de Hoces et al. 2010). The calculated  $t_{50}$  values are similar to those acquired experimentally.

By analyzing the parameters of BDST model, the volumetric adsorption capacity,  $N_0$ , decreases with increasing flow rate and bed depth (Muhamad et al. 2010).

**Table 4** Thomas, Yoon–Nelson, Clark, dose–response, and BDST model parameters

Model parameters	Unity	Exp. no.						
		1	2	3	4	5	6	7
<b>Thomas</b>								
$K_{Th}$	$m^3 g^{-1} min^{-1}$	0.091	0.060	0.069	0.078	0.067	0.075	0.043
$q_0$	$mg g^{-1}$	6.872	5.465	4.581	6.161	4.693	5.634	4.319
$R^2$	–	0.999	0.998	0.998	0.999	0.994	0.997	0.998
<b>Yoon–Nelson</b>								
$K_{YN}$	$min^{-1}$	0.454	0.3809	0.443	0.683	0.740	0.482	0.275
$t_{50}$	min	17.043	20.330	23.097	14.770	6.705	19.562	24.994
$t_{50 \text{ experience}}$	min	17.042	20.351	23.094	14.792	6.754	19.418	25.024
$R^2$	–	0.999	0.998	0.998	0.999	0.994	0.997	0.998
<b>Clark</b>								
$A$	–	3880	3875	53,609	45,408	214	2289	1600
$r$	–	0.474	0.397	0.463	0.714	0.773	0.504	0.288
$n$	–	2.128	2.128	2.128	2.128	2.128	2.128	2.128
$R^2$	–	0.999	0.998	0.998	0.999	0.994	0.997	0.998
<b>Dose–response</b>								
$q_0$	$mg g^{-1}$	6.801	5.272	4.629	6.111	4.581	5.595	4.262
$a$	–	7.808	6.352	10.135	10.099	4.908	9.336	6.861
$R^2$	–	0.994	0.999	0.999	0.999	0.994	0.997	0.997
<b>BDST</b>								
$K_{BDST}$	$m^3 g^{-1} min^{-1}$	0.091	0.060	0.069	0.078	0.0666	0.075	0.043
$N_0$	$g m^{-3}$	135.667	107.886	91.926	161.110	92.6469	218.108	464.997
$R^2$	–	0.999	0.998	0.998	0.999	0.994	0.997	0.998

In previous study (Dammak et al. 2014), Freundlich model was found to be valid for the adsorption of *o*-xylene, so the Freundlich constant obtained ( $n = 2.128$ ) was used as parameter in Clark model. As seen in Table 4, as inlet *o*-xylene concentration increased, the values of  $r$  increased.

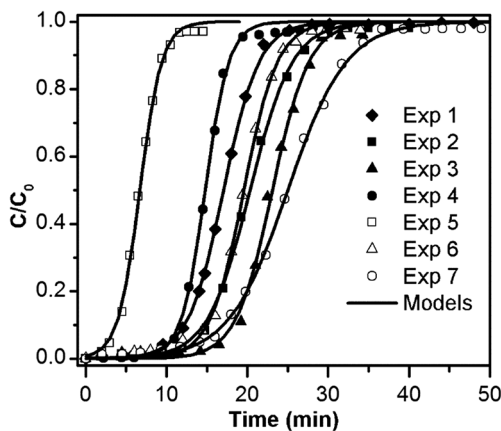


**Fig. 4** Experimental and total breakthrough model curves for *o*-xylene onto clay material at different flow rates, bed heights, and inlet *o*-xylene concentrations.  $0.3 \times 10^{-3} m^3 min^{-1}$ , 0.1 m,  $6.4 g m^{-3}$  (diamonds);  $0.63 \times 10^{-3} m^3 min^{-1}$ , 0.15 m,  $6.4 g m^{-3}$  (filled squares);  $0.63 \times 10^{-3} m^3 min^{-1}$ , 0.2 m,  $6.4 g m^{-3}$  (filled triangles);  $0.63 \times 10^{-3} m^3 min^{-1}$ , 0.1 m,  $8.77 g m^{-3}$  (filled circles);  $0.63 \times 10^{-3} m^3 min^{-1}$ , 0.1 m,  $11.11 g m^{-3}$  (empty squares);  $0.45 \times 10^{-3} m^3 min^{-1}$ , 0.1 m,  $6.4 g m^{-3}$  (empty triangles);  $0.27 \times 10^{-3} m^3 min^{-1}$ , 0.1 m,  $6.4 g m^{-3}$  (empty circles)

For all cited models, the correlation between the experimental and calculated data is not affected by the variation of parameters.

**Advection–dispersion–sorption model**

The simple models for adsorption in the columns (BDST, Thomas, Yoon–Nelson, etc.) fit experimental results fairly well. However, in order to obtain the transport parameters, another model based on the mass transfer has been developed. The mass balance led to the following second-order partial differential equation:

$$-D_{ax} \frac{\partial^2 C}{\partial Z^2} + v \frac{\partial C}{\partial Z} + \frac{\partial C}{\partial t} + \frac{(1-\epsilon)\rho}{\epsilon} \frac{\partial q}{\partial t} = 0 \tag{12}$$

The initial conditions are at  $t = 0$   $\begin{cases} C(Z, 0) = 0 \\ q(Z, 0) = 0 \end{cases}$ .

The boundary conditions are  $\begin{cases} Z = 0 \Rightarrow C(0, t) = C_0 \\ Z = L \Rightarrow \frac{\partial C}{\partial Z} = 0 \end{cases}$ .

Equation (12) is composed of four terms: the first describes axial dispersion, the second is an advection term, the third depicts the accumulation in fluid phase, and the fourth represents the accumulation in the solid phase. The resolution of Eq. (12), with initial and boundary conditions, leads to the solution of the problem of the fixed-bed adsorption.

Solution 1

Assuming a plug flow, we can neglect the axial dispersion (Simo et al. 2008). Modeling transport equations in a packed column depends greatly on the mechanism by which the mass transfer of solid–fluid occurs. External mass transfer is the diffusion of the solute through the boundary layer surrounding the adsorbent particle, whereas internal mass transfer is the diffusion within the porous network. Therefore, in the modeling of a column, the effects of mass transfer resistance, between the fluid and the particle on one hand and within the particle on the other hand, should be considered (Rutherford and Do 2000a, 2000b; Afzal et al. 2010; Leinekugel-le-Cocq et al. 2007). Glueckauf law is used to describe the internal mass transfer. Linear model was used to describe the adsorption isotherm.

$$(S_1) \begin{cases} v \frac{\partial C}{\partial Z} + \frac{\partial C}{\partial t} + \frac{(1-\varepsilon)}{\varepsilon} \rho \frac{\partial q}{\partial t} = 0 & \text{Mass transfer balance} \\ \frac{\partial q}{\partial t} = \frac{k_f \times a_p}{\rho} \times (C - C_i) & \text{External diffusion} \\ \frac{\partial q}{\partial t} = k_s \times a_p \times (q_i - q) & \text{Internal diffusion (Glueckauf)} \\ q_i = k \times C & \text{Adsorption isotherm (Linear)} \end{cases} \quad (13)$$

with  $a_p = \frac{6(1-\varepsilon)}{d_p}$  and  $K_S = k_s \times a_p = \frac{60 \times D_{eff}}{d_p^2}$ .

To solve Eq. (3), the term  $(\frac{\partial q}{\partial t})$  must be calculated by combining equations of the system (S<sub>1</sub>). We assume that the adsorption kinetics is controlled by both external and internal diffusion.

Posing  $x = \frac{C}{C_0}$ ;  $z = \frac{Z}{L}$ ;  $A_1 = \frac{v}{L} = \frac{u}{L \times \varepsilon}$ ;  $A_2 = \frac{\rho \times (1-\varepsilon)}{\varepsilon \times C_0}$ ;  $K_G = \frac{k_f \times a_p \times C_0}{\rho}$ ;  $K_S = k_s \times a_p = \frac{15 \times D_{eff}}{R_p^2}$  and  $K = k \times C_0$ , the system of equations (S<sub>1</sub>) becomes

$$(S_1) \begin{cases} \frac{\partial x}{\partial t} = -A_1 \left( \frac{\partial x}{\partial z} \right) - A_2 \left( \frac{\partial q}{\partial t} \right) \\ \frac{\partial q}{\partial t} = K_G \times \left( x - \left( \frac{K_S \times x + K_S \times q}{K_S \times K + K_G} \right) \right) \end{cases} \quad (14)$$

---


$$(S_2) \begin{cases} \frac{\partial x}{\partial t} = -A_1 \left( \frac{\partial x}{\partial z} \right) - A_2 \left( \frac{\partial q}{\partial t} \right) \\ \frac{\partial q}{\partial t} = K_G \left[ \frac{x}{2} - \frac{q}{2 \times a_0} + a_1 - a_2 \sqrt{(a_3 - b(a_0 \times x + q))^2 + 4 \times b \times a_0(q + a_0 \times x)} \right] \end{cases} \quad (16)$$


---

Initial conditions  $\begin{cases} t = 0 \\ x(z, 0) = 0 \\ q(z, 0) = 0 \end{cases}$

Boundary conditions  $\begin{cases} z = 0 \Rightarrow x(0, t) = 1 \\ z = 1 \Rightarrow \frac{\partial x}{\partial z} = 0 \end{cases}$

Initial conditions  $\begin{cases} t = 0 \\ x(z, 0) = 0 \end{cases} \quad q(z, 0) = 0.$

Boundary conditions  $\begin{cases} z = 0 \Rightarrow x(0, t) = 1 \\ z = 1 \Rightarrow \frac{\partial x}{\partial z} = 0 \end{cases}$

The mass transfer models were modeled using COMSOL 4.2 software. The solution 1, described in Fig. 5, shows a deviation from the experimental data ( $R^2 = 0.203$ ). The parameters obtained from mathematical modeling of this solution are given in Table 5. The use of a linear isotherm does not describe the experience properly. Therefore, adsorption isotherm of clay and *o*-xylene is nonlinear. Improved analytic solution for the system can be obtained using Langmuir isotherm.

Solution 2

For this solution, the differential equation system (S<sub>2</sub>) is composed of the same equations than those of (S<sub>1</sub>); only the adsorption isotherm equation becomes the nonlinear equation of Lagmuir.

$$(S_2) \begin{cases} v \frac{\partial C}{\partial Z} + \frac{\partial C}{\partial t} + \frac{(1-\varepsilon)}{\varepsilon} \rho \frac{\partial q}{\partial t} = 0 & \text{Mass transfer balance} \\ \frac{\partial q}{\partial t} = \frac{k_f \times a_p}{\rho} \times (C - C_i) & \text{External diffusion} \\ \frac{\partial q}{\partial t} = k_s \times a_p \times (q_i - q) & \text{Internal diffusion (Glueckauf)} \\ q_i = \frac{q_0 \times K_L \times C_i}{1 + K_L \times C_i} & \text{Adsorption isotherm (Langmuir)} \end{cases} \quad (15)$$

Posing  $a = q_0 \times K_L \times C_0$ ;  $b = K_L \times C_0$ ;  $a_0 = \frac{K_G}{K_S}$ ;  $a_1 = \frac{a}{2 \times b \times a_0} + \frac{1}{2 \times b}$ ;  $a_2 = \frac{1}{2 \times b \times a_0}$  and  $a_3 = a + a_0$ , the final system (S<sub>2</sub>) of differential equations to be solved, using the nonlinear Langmuir isotherm, is the following:

The second solution is approaching the experience and describes it with a correlation coefficient value  $R^2 = 0.972$  (Fig. 5). According to this figure, the deviation between experimental and simulated breakthrough is observed in this range, which is specific to our experiments. To further improve the internal transfer



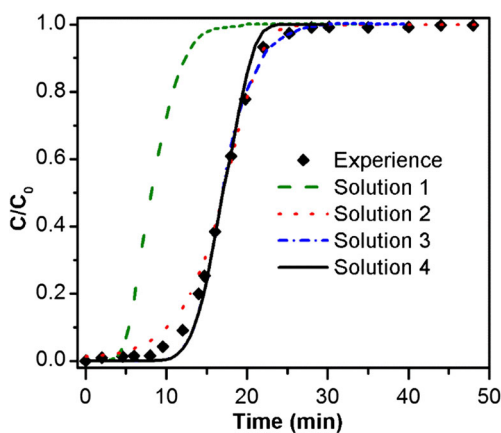


**Fig. 5** The four solutions for the mass transfer model breakthrough curves for *o*-xylene onto clay material;  $0.63 \times 10^{-3} \text{ m}^3 \text{ min}^{-1}$ , 0.1 m,  $6.4 \text{ g m}^{-3}$  (diamonds)

model, Rosen law was used to describe the transfer within the means radius of particle  $R_p$ .

*Solution 3*

The differential equation system of solution 3 consists of the mass balance, the external mass transfer equation, the internal mass transfer equation (Rosen law), and the adsorption isotherm (Langmuir model).

$$(S_3) \begin{cases} v \frac{\partial C}{\partial Z} + \frac{\partial C}{\partial t} + \frac{(1-\varepsilon)}{\varepsilon} \rho \frac{\partial q}{\partial t} = 0 & \text{Mass transfer balance} \\ \frac{\partial q}{\partial t} = \frac{k_f \times a_p}{\rho} \times (C - C_i) & \text{External diffusion} \\ \frac{\partial q_j}{\partial t} = D_{\text{eff}} \left( \frac{\partial^2 q_j}{\partial r^2} + \frac{2}{r} \frac{\partial q_j}{\partial r} \right) & \text{Internal diffusion (Rosen)} \\ q_i = \frac{q_0 \times K_L \times C_i}{1 + K_L \times C_i} & \text{Adsorption isotherm (Langmuir)} \end{cases} \quad (17)$$

The description of the adsorption phenomenon within the particle is described by the Rosen model.

**Table 5** Mass transfer model parameters

Model parameters	unity	Exp. no.						
		1	2	3	4	5	6	7
Mass transfer model								
$K_S$	$\text{s}^{-1}$	0.0228	0.0228	0.0228	0.0252	0.0255	0.0228	0.0228
$K_G$	$\text{m}^3 \text{ kg}^{-1} \text{ s}^{-1}$	0.0015	0.0015	0.0015	0.0022	0.0027	0.0013	0.00098
$q_0$	$\text{g g}^{-1}$	0.0284	0.0255	0.0247	0.0250	0.0132	0.0239	0.0224
$K_L$	–	13.094	4.850	2.806	10.067	5.067	8.067	2.572
$k$	–	0.531	0.759	0.716	0.719	0.162	0.705	0.813

Posing  $\xi = \frac{r}{R_p}; k_1 = \frac{3 \times D_{\text{eff}} \times A_2}{R_p^2}; k_2 = \frac{D_{\text{eff}}}{R_p \times k_f}$ , the final system ( $S_3$ ) of differential equations to be solved, is the following:

$$(S_3) \begin{cases} \frac{\partial x}{\partial t} = -A_1 \left( \frac{\partial x}{\partial z} \right) - \frac{3 \times D_{\text{eff}} \times A_2}{R_p^2} \frac{\partial q_j}{\partial \xi} \Big|_{\xi=1} \\ \frac{\partial q_j}{\partial t} = \frac{D_{\text{eff}}}{R_p^2} \left( \frac{\partial^2 q_j}{\partial \xi^2} + \frac{2}{\xi} \frac{\partial q_j}{\partial \xi} \right) \end{cases} \quad (18)$$

with

$$\begin{cases} q_j(z, \xi, 0) = 0 \\ q_j(z, 1, t) = \frac{a \times x(z, t) - a \times k_2 \frac{\partial q_j(z, 1, t)}{\partial \xi}}{1 + b \times x(z, t) - b \times k_2 \frac{\partial q_j(z, 1, t)}{\partial \xi}} \\ \frac{\partial q_j(z, 0, t)}{\partial \xi} = 0 \end{cases} \quad (19)$$

The model coincides with experience (Fig. 5); the theory balance revealed a narrow gap with the experimental data ( $R^2 = 0.988$ ). In addition, the staggering of breakthrough fronts, which corresponds to kinetic effects of mass transfer, is also well represented by theoretical calculations. The simulation shows a difference in concentration of *o*-xylene at the outlet of the column which can be attributed to the dispersion term. Therefore, we will take action in solution 4 for quite satisfactory results.

*Solution 4*

In an attempt to build a theoretical representation that approximates as closely as possible to a real process, we took into account the effects of the axial dispersion. This is necessary when the ratio (length bed/particle diameter) is greater than 30 (Cloirec 2003). In our case, the minimum bed length is 100 mm and the diameter of the particle is 0.85 mm ( $L_c/d_p$ .

= 117). The axial dispersion coefficient is calculated using Eq. (20) (Ho and Webb 2006; Edward and Richardson 1968).

$$D_{ax} = 0.73 \times D_m + \frac{v \times R_p}{1 + \frac{9.7 \times D_m}{2 \times v \times R_p}} \quad (20)$$

Differential equation system then is composed from the mass balance taking into account the axial dispersion, the external mass transfer equation, the internal mass transfer equation (Rosen law), and the adsorption isotherm (Langmuir model).

$$(S_4) \begin{cases} -D_{ax} \frac{\partial^2 C}{\partial Z^2} + v \frac{\partial C}{\partial Z} + \frac{\partial C}{\partial t} + \frac{(1-\varepsilon)}{\varepsilon} \rho \frac{\partial q}{\partial t} = 0 & \text{Mass transfer balance} \\ \frac{\partial q}{\partial t} = \frac{k_f \times a_p}{\rho} \times (C - C_i) & \text{External diffusion} \\ \frac{\partial q_j}{\partial t} = D_{eff} \left( \frac{\partial^2 q_j}{\partial r^2} + \frac{2}{r} \frac{\partial q_j}{\partial r} \right) & \text{Internal diffusion (Rosen)} \\ q_i = \frac{q_0 \times K_L \times C_i}{1 + K_L \times C_i} & \text{Adsorption isotherm (Langmuir)} \end{cases} \quad (21)$$

Posing  $A_3 = \frac{D_{ax}}{L^2}$ , the final system ( $S_4$ ) of differential equations to be solved is the following:

$$(S_4) \begin{cases} \frac{\partial x}{\partial t} = A_3 \left( \frac{\partial^2 x}{\partial z^2} \right) - A_1 \left( \frac{\partial x}{\partial z} \right) - \frac{3 \times D_{eff} \times A_2}{R_p^2} \frac{\partial q_j}{\partial \xi} \Big|_{\xi=1} \\ \frac{\partial q_j}{\partial t} = \frac{D_{eff}}{R_p^2} \left( \frac{\partial^2 q_j}{\partial \xi^2} + \frac{2}{\xi} \frac{\partial q_j}{\partial \xi} \right) \end{cases} \quad (22)$$

Taking into account the term of axial dispersion, the mass transfer model is close to the experience and describes well the breakthrough ( $R^2 = 0.996$ ). This is favorable both on the shape of the simulated curves (Fig. 5) and on the numerical results of the adsorbed amounts (Table 5). Experiments that have been conducted in these conditions can be reproduced correctly by simulation. The comparison between the experimental and model predicted curves gives rise to the conclusion that the mass transfer model (solution 4) is able to predict the column behavior with a good degree of accuracy.

Bed depth, inlet concentration, and gas flow variations obtained with COMSOL describe well the experimental results. In addition, the staggering breakthrough curves match at a time kinetic effects of a transfer material, were well represented by the theoretical calculations.

The mass transfer model provides more information than the other models. The rate constant ( $k_f$ ) includes both a diffusion term ( $D_{eff}$ ) and velocity term ( $v$ ), which are important in scaling up the size of the column (depth and diameter) and maximizing the flow rate for efficiency. The difference between internal and external surface areas is accounted for using both total surface area ( $a_p$ ) and porosity ( $\varepsilon$ ).

It is clear that the model captures the essential physics of mass transfer inside the column. Thus, this model relates more parameters about the column than the other models, which is more useful in optimizing the column size, flow rate, and particle characteristics. The fact that we obtain a good agreement between the proposed model and the experimental data for a large range of configurations is a very strong argument in favor of the theory.

### Industrial extrapolation

The aim of this study is to use raw clay material as adsorbent in industry. Laboratory experiments are carried out under special conditions where the majority of parameters are very well controlled.

In an industrial application, some parameters will have a greater range of variation than in the laboratory, since larger quantities will be deployed. Indeed, the density, the particle size (directly affecting  $K_L$ ), and the axial dispersion are the parameters which are difficult to control.

The objective of the industrial extrapolation section is to simulate the behavior of the adsorption fronts when density ( $\rho$ ), Langmuir constant ( $K_L$ ), and axial dispersion ( $D_{ax}$ ) are varied. We purposely chose to enlarge the range of variation of each parameter (10, 20, and 30%) probably much more than it is usually tolerated using experimental design.

A central composite matrix was used (Table 6). The adsorption front (response) will be determined by simulation on COMSOL (and not experimentally). A theoretical model will be established according to the three parameters. We develop in this part a study of the experimental error effect, for various experimental parameters on the adsorption breakthrough.

**Table 6** Central composite design matrix for three variables and response results

Run no.	Simulation design			Factors			Breakthrough time			
				$\rho$ (kg m <sup>-3</sup> )	$K_L$ (-)	$D_{ax}$ (m <sup>2</sup> s <sup>-1</sup> )	Simulated (s)	Predicted (s)	Residues (s)	Residues (%)
1	-1	-1	-1	1250	10.62	83.3	517	526.4	-9.4	-1.79
2	1	-1	-1	1530	10.62	83.3	640	652.1	-12.1	-1.86
3	-1	1	-1	1250	15.94	83.3	554	546.6	7.4	1.35
4	1	1	-1	1530	15.94	83.3	681	678.3	2.7	0.40
5	-1	-1	1	1250	10.62	154.7	466	474.5	-8.5	-1.79
6	1	-1	1	1530	10.62	154.7	576	589.2	-13.2	-2.24
7	-1	1	1	1250	15.94	154.7	501	494.7	6.3	1.27
8	1	1	1	1530	15.94	154.7	619	615.4	3.6	0.58
9	-1	0	0	1250	13.28	119.0	587	582.9	4.1	0.70
10	1	0	0	1530	13.28	119.0	725	706.1	18.9	2.68
11	0	-1	0	1390	10.62	119.0	632	588.9	43.1	7.32
12	0	1	0	1390	15.94	119.0	592	612.1	-20.1	-3.28
13	0	0	-1	1390	13.28	83.3	603	591.7	11.3	1.91
14	0	0	1	1390	13.28	154.7	546	534.3	11.7	2.19
15	0	0	0	1390	13.28	119.0	572	618.0	-46.0	-7.44

Simulated breakthrough time: calculated from mass balance equations with COMSOL, based on experimental results. Predicted breakthrough time: determined from the theoretical model (Eq. 23)

*Parameter choice*

The density of the clay material is a parameter which greatly influences the breakthrough front time, and it cannot be determined experimentally. We have tolerated  $\pm 10\%$  as margin of error.

Physical adsorption of *o*-xylene on the clay material is exothermic: at high temperature, the slope of the adsorption isotherm is stiff, which reduces the Langmuir

constant  $K_L$ . We have tolerated  $\pm 20\%$  as margin of error.

$D_{ax}$  is a function of the diameter of the particle, the porosity of the bed, and the adsorption temperature, so these parameters influence the breakthrough time. During the determination of  $D_{ax}$ , we have tolerated a margin of error of  $\pm 30\%$ .

In this part, we have to optimize the breakthrough time in order to minimize the number of adsorption/desorption cycles in an industrial application.

**Table 7** Coefficient model estimation for breakthrough time response

Parameter	Coef	Coef value	SD	t. test	Student test (t)	P-Value
$X_1$	$b_1$	61.6	10.6	5.82		0.263**
$X_2$	$b_2$	11.6	10.6	1.10		32.4
$X_3$	$b_3$	-28.7	10.6	-2.71		4.19
$X_1 \times X_2$	$b_{12}$	1.5	11.8	0.13		90.0
$X_1 \times X_3$	$b_{13}$	-2.7	11.8	-0.23		81.9
$X_2 \times X_3$	$b_{23}$	0.0	11.8	0.00		100.0
$X_1^2$	$b_{11}$	26.6	20.9	1.27		25.9
$X_2^2$	$b_{22}$	-17.4	20.9	-0.84		44.5
$X_3^2$	$b_{33}$	-54.9	20.9	-2.63		4.60*

SD standard deviation

\*\*Significant to 99%; \*Significant to 95%

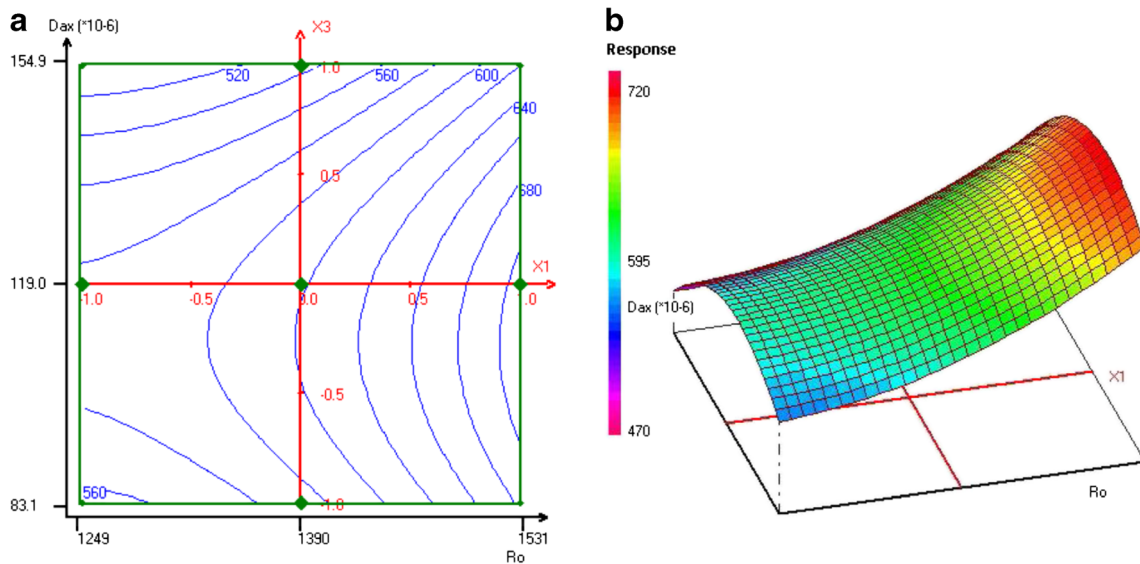


**Fig. 6** Variation of breakthrough time versus  $\rho$  and  $D_{ax}$  at  $K_L = 13.281$

*Modeling*

The response,  $\hat{Y}$ , can be calculated from  $X_1$ ,  $X_2$ , and  $X_3$  by a quadratic regression model.

$$\begin{aligned}
 Y = & 618.0 + 61.60X_1 + 11.60X_2 - 28.70X_3 \\
 & + 26.60X_1^2 - 17.40X_2^2 - 54.90X_3^2 \\
 & + 1.50X_1X_2 - 2.70X_1X_3 + 0.00X_2X_3 \quad (23)
 \end{aligned}$$

The simulated values are obtained by simulation of mass balance equation with COMSOL MULTIPHYSICS. These values replace the experimental data in this section.

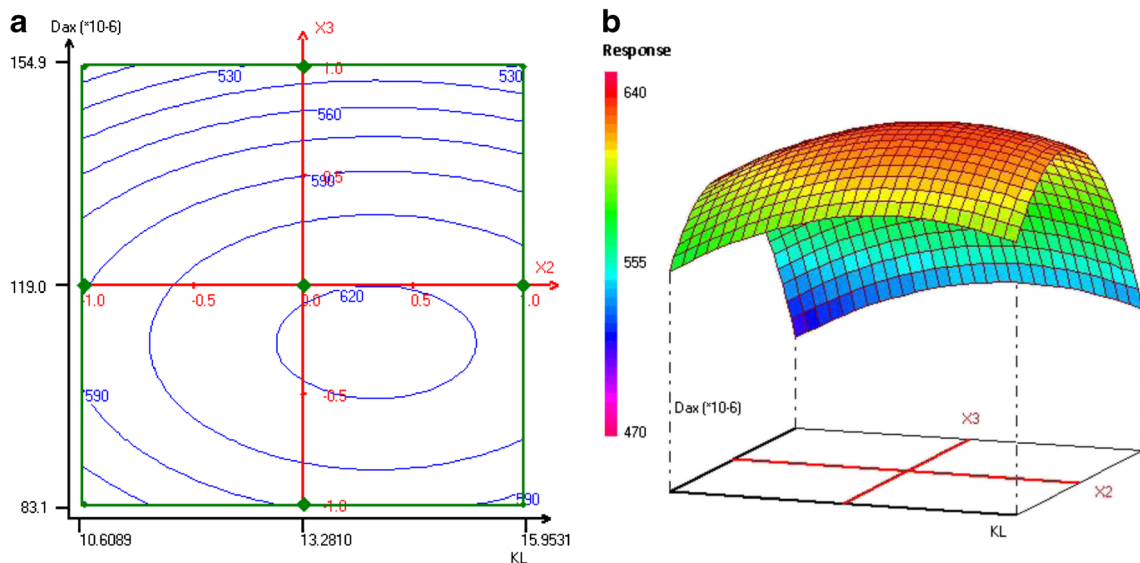
Therefore, predicted values are those determined by NEMROD.

Table 6 shows the simulation design of clay material based on the variables  $\rho$ ,  $K_L$ , and  $D_{ax}$  for breakthrough time response obtained by mass balance equation model. Predicted breakthrough time and residues are also presented in this table.

The significance of each coefficient of quadratic regression model is determined by Student's *t* tests, which are listed in the Table 7.

The validation of the quadratic regression model was reanalyzed by using residuals. Residuals were distributed normally with mean zero and constant variance.

The correlation coefficient value  $R^2 = 0.913$  justifies an excellent relation (Table 6) between the independent variables



**Fig. 7** Variation of breakthrough time versus  $K_L$  and  $D_{ax}$  at  $\rho = 1390 \text{ kg m}^{-3}$

**Table 8** Desirability: maximum coordinates

Variable	Value	Factor	Value
$X_1$	1.000	$\rho$ (kg m <sup>-3</sup> )	1530
$X_2$	0.375	$K_L$	14.2783
$X_3$	-0.286	$D_{ax}$ ( $\times 10^{-6}$ ) (m <sup>2</sup> s <sup>-1</sup> )	108.8
Desirability	0.862	Breakthrough time (s)	713.1

and good agreement between the simulated and predicted model (Amari et al. 2008).

It was concluded that Eq. (20) was good to fit to the simulated data. In other words, the assumptions regarding the errors are satisfactory.

The coefficients of the suggested model were calculated according to the experimental responses and the iso-response curves (Table 7). To evaluate the response and interpret the results, these coefficients were used. Therefore, it is needed to predict the effect of each factor and their interactions which can be synergistic or antagonistic.

The greater the amplitude of the  $t$  value, the greater the corresponding coefficient is important (Akhnazarova and Kafarov 1982; Khuri and Cornell 1996). Thus, the linear effects of density and Langmuir constant are very significant, as is evident from the Student's  $t$  test values (Table 7). The effect of interactions is considered insignificant at the 95% confidence level.

The effect sign marks the breakthrough time. For a response factor, a synergistic effect is designated by a positive sign, whereas an antagonistic effect is designated by a negative sign (Haaland 1989).

As shown in Table 7 and in the model coefficients (18), it was concluded that absolute value of linear effect was more significant than quadratic effects.

The linear effects of  $\rho$  and  $K_L$  factors are positive (61.6 and 11.6), whereas that of  $D_{ax}$  factor is negative (-28.7): an increase in  $\rho$  and  $K_L$  during the adsorption is accompanied with an increase in breakthrough time; the same result is obtained for a decrease in  $D_{ax}$ . All quadratic effects, except of density, are negative: the increase in the axial dispersion in the column does not affect breakthrough time generally. The mutual effect ( $X_i X_j$  with  $i \neq j$ ) was found to be the least significant effect of all the other factor effects. The mutual effect can be seen in an elliptical shape in proportional with its significance in Figs. 6 and 7. To increase the breakthrough time, variable values should be with same sign.

It is easy to note that the breakthrough time can be maximized when the density of clay is maximized, while the effect of the Langmuir constant and the axial dispersion effect are less important.

In order to visualize the relationship between the simulated variables and the response, we represented the 2D iso-response curves and 3D response surface (Figs. 6 and 7). Each area represented by these figures is a combination of

two variables; the other parameters are kept constant at the point center.

The desirability function is the relationship between the expected responses of dependent variable and their desirability. It is based on the assignment of values from 0 (not desirable) and 1 (highly desirable) to the expected response. With desirability function, the values of the dependent variables that produce the most desirable responses can be determined. If the combination of answers is optimal, desirability will have a high value.

A study of the desirability function was performed in order to maximize the breakthrough time. In Table 8, optimal independent variables are enumerated. These values show that with a density of 1530 g cm<sup>-3</sup>, Langmuir constant of 14.28, and a dispersion coefficient of  $108.8 \times 10^{-6}$  m<sup>2</sup> s<sup>-1</sup>, there will be a desirability of 0.862 and a breakthrough time of 713 s.

### Conclusions

This study verified that the raw clay material can be used as adsorbent for the treatment of volatile organic compounds.

Dynamic experiments marked the importance of bed height, inlet *o*-xylene concentration, and flow rate. Decreasing bed height and inlet *o*-xylene concentration enhanced column performance, whereas, the highest flow rate raised adsorption capacity. It has also been demonstrated that column data could be perfectly described by the Thomas, Yoon–Nelson, Clark, dose–response, and BDST models. Moreover, mass transfer model provides a description of the experimental results at different bed heights, flow rate, and inlet *o*-xylene concentrations.

**Acknowledgements** The authors are grateful to PHC Maghreb no. 27959PD for financial support.

### References

- Acheampong MA, Pakshirajan K, Annachatre AP, Lens PNL (2013) Removal of Cu (II) by biosorption onto coconut shell in fixed-bed column systems. *J Ind Eng Chem* 19:841–848
- Afzal S, Rahimi A, Ehsani MR, Tavakoli H (2010) Modeling hydrogen fluoride adsorption by sodium fluoride. *J Ind Eng Chem* 16:978–985
- Akhnazarova S, Kafarov V (1982) Experiment optimization in chemistry and chemical engineering. Mir Publishers, Moscow
- Aksu Z, Gönen F (2006) Binary biosorption of phenol and chromium (VI) onto immobilized activated sludge in a packed bed: prediction of kinetic parameters and breakthrough curves. *Sep Purif Technol* 49:205–216
- Amari A, Gannouni A, Chlendi M, Bellagi A (2008) Optimization by response surface methodology (RSM) for toluene adsorption onto prepared acid activated clay. *Can J Chem Eng* 86:1093–1102
- Bohart GS, Adams EQ (1920) Some aspects of the behaviour of the charcoal with respect chlorine. *J Am Chem Soc* 42:523–544
- Calero de Hocés M, Blázquez García G, Ronda Gálvez A, Martín-Lara MA (2010) Effect of the acid treatment of olive stone on the biosorption of lead in a packed-bed column. *Ind Eng Chem Res* 49:12587–12595

- Calero M, Hernáinz F, Blázquez G, Tenorio G, Martín-Lara MA (2009) Study of Cr (III) biosorption in a fixed-bed column. *J Hazard Mater* 171:886–893
- Chafik T, Harti S, Cifredo G, Gatica JM, Vidal H (2009) Easy extrusion of honeycomb-shaped monoliths using Moroccan natural clays and investigation of their dynamic adsorptive behavior towards VOCs. *J Hazard Mater* 170:87–95
- Chen N, Zhang Z, Feng C, Li M, Chen R, Sugiura N (2011) Investigations on the batch and fixed-bed column performance of fluoride adsorption by Kanuma mud. *Desalination* 268:76–82
- Chu KH (2004) Improved fixed bed models for metal biosorption. *Chem Eng J* 97(2–3):233–239
- Clark RM (1987) Evaluating the cost and performance of field-scale granular activated carbon systems. *Environ Sci Technol* 21:573–580
- Cloirec PL (2003) Adsorption en traitement de l'air. *Techniques de l'ingénieur G1 770:13*
- Dammak N, Fakhfakh N, Fourmentin S, Benzina M (2013) Natural clay as raw and modified material for efficient o-xylene abatement. *J Env Chem Eng* 1:667–675
- Dammak N, Fakhfakh N, Fourmentin S, Benzina M (2015) Treatment of gas containing hydrophobic VOCs by adsorption process on raw and intercalated clays. *Res Chem Intermed* 41:5475–5493
- Dammak N, Ouledtaif O, Fakhfakh N, Benzina M (2014) Adsorption equilibrium studies for oxylyene vapour and modified clays system. *Surf Interface Anal* 46:457–464
- Edward MF, Richardson JF (1968) Gas dispersion in packed beds. *Chem Eng Sci* 23:109–123
- Guibal E, Lorenzelli R, Vincent T, Cloirec L (1995) Application of silica gel to metal ion sorption: static and dynamic removal of uranyl ions. *Environ Technol* 16:101–114
- Gupta VK, Verma N (2002) Removal of volatile organic compounds by cryogenic condensation followed by adsorption. *Chem Eng Sci* 57:2679–2696
- Haaland PD (1989) Separating signals from the noise in experimental design in biotechnology. Marcel Dekker, New York, pp 61–83
- Hamdaoui O (2006) Dynamic sorption of methylene blue by cedar sawdust and crushed brick in fixed bed columns. *J Hazard Mater* 138:293–303
- Han R, Ding D, Xu Y, Zou W, Wang Y, Li Y, Zou L (2008) Use of rice husk for the adsorption of congo red from aqueous solution in column mode. *Bioresour Technol* 99:2938–2946
- Han RP, Zou LN, Zhao X, Xu YF, Xu F, Li YL, Wang Y (2009) Characterization and properties of iron oxide-coated zeolite as adsorbent for removal of copper (II) from solution in fixed bed column. *Chem Eng J* 149:123–131
- Hasan SH, Ranjan D, Talat M (2010) Agro-industrial waste 'wheat bran' for the biosorptive remediation of selenium through continuous up-flow fixed-bed column. *J Hazard Mater* 181:1134–1142
- Ho CK, Webb SW (eds) (2006) Gas transport in porous media. Springer, Dordrecht
- Huang S, Zhang C, He H (2009) In situ adsorption-catalysis system for the removal of o-xylene over an activated carbon supported Pd catalyst. *J Environ Sci* 21:985–990
- Huang ZH, Kang F, Liang KM, Hao J (2003) Breakthrough of methylethylketone and benzene vapors in activated carbon fiber beds. *J Hazard Mater* 98:107–115
- Jones AP (1999) Indoor air quality and health. *Atmos Environ* 33(28):4535–4564
- Khuri AI, Cornell JA (1996) Response surfaces: design and analysis, 2nd edn. Marcel Dekker, New York
- Ko DCK, Porter JF, McKay G (2000) Optimised correlations for the fixed bed adsorption of metal ions on bone char. *Chem Eng Sci* 55:5819–5829
- Kumar PA, Chakraborty S (2009) Fixed-bed column study for hexavalent chromium removal and recovery by short-chain polyaniline synthesized on jute fiber. *J Hazard Mater* 162:1086–1098
- Lee JF, Mortland MM, Chiou CT, Kile DE, Boyd SA (1990) Adsorption of benzene, toluene, and xylene by two tetramethylammonium-smectites having different charge densities. *Clay Clay Miner* 38(2):113–120
- Leinekugel-le-Cocq D, Tayakout-Fayolle M, Le Gorrec Y, Jallut C (2007) A double linear driving force approximation for non-isothermal mass transfer modeling through bi-disperse adsorbents. *Chem Eng Sci* 62:4040–4053
- Leyva-Ramos R, Diaz-Flores PE, Leyva-Ramos J, Femat-Flores RA (2007) Kinetic modeling of pentachlorophenol adsorption from aqueous solution on activated carbon fibers. *Carbon* 45:2280–2289
- Lin SH, Cheng MJ (2002) Adsorption of phenol and m-chlorophenol on organo bentonites and repeated thermal regeneration. *Waste Manag* 22:595–603
- Lua AC, Jandia QP (2009) Adsorption of phenol by oil-palm-shell activated carbons in a fixed bed. *Chem Eng J* 150:455–461
- Malek A, Farooq S (1997) Kinetics of hydrocarbon adsorption on activated carbon and silica gel. *AIChE J* 43:761–776
- Minceva M, Rodrigues AE (2004) Adsorption of xylenes on faujasite-type zeolite equilibrium and kinetics in batch adsorber. *Chem Eng Res and Des* 82(A5):667–681
- Morales Futulan C, Kan CC, Dalida ML, Pascua C, Wan WW (2011) Fixed-bed column studies on the removal of copper using chitosan immobilized on bentonite. *Carbohydr Polym* 83:697–704
- Muhamad H, Doan H, Lohi A (2010) Batch and continuous fixed-bed column biosorption of Cd<sup>2+</sup> and Cu<sup>2+</sup>. *Chem Eng J* 158:369–377
- Pires J, Carvalho A, De Carvalho MB (2001) Adsorption of volatile organic compounds in Y zeolites and pillared clays. *Micropor Mesopor Mater* 43:277–287
- Qaiser S, Saleemi AR, Umar M (2009) Biosorption of lead from aqueous solution by *Ficus religiosa* leaves: batch and column study. *J Hazard Mater* 166:998–1005
- Rao KS, Anad S, Venkateswarlu P (2011) Modeling the kinetics of Cd(II) adsorption on *Syzygiumcumini* L. leaf powder in a fixed bed mini column. *J Ind Eng Chem* 17:174–181
- Rutherford SW, Do DD (2000a) Adsorption dynamics measured by permeation and batch adsorption methods. *Chem Eng J* 76:23–31
- Rutherford SW, Do DD (2000b) Adsorption dynamics of carbon dioxide on a carbon molecular sieve 5A. *Carbon* 38:1339–1350
- Sarin V, Singh TS, Pant KK (2006) Thermodynamic and breakthrough column studies for the selective sorption of chromium from industrial effluent on activated eucalyptus bark. *Bioresour Technol* 97:1986–1993
- Simo M, Brown CJ, Hlavacek V (2008) Simulation of pressure swing adsorption in fuel ethanol production process. *Comput Chem Eng* 32:1635–1649
- Thomas HC (1944) Heterogeneous ion exchange in a flowing system. *J Am Chem Soc* 66:1664–1666
- Tor A, Danaoglu N, Arslan G, Cengeloglu Y (2009) Removal of fluoride from water by using granular red mud: batch and column studies. *J Hazard Mater* 164:271–278
- Vijayaraghavan K, Prabu D (2006) Potential of *Sargassum wightii* biomass for copper (II) removal from aqueous solutions: application of the different mathematical models to batch and continuous biosorption data. *J Hazard Mater* 137:558–564
- Vinodhini V, Das N (2010) Packed bed column studies on Cr (VI) removal from tannery wastewater by neem sawdust. *Desalination* 264:9–14
- Wolborska A (1989) Adsorption on activated carbon of p-nitrophenol from aqueous solution. *Water Res* 23:85–91
- Yan GY, Viraraghavan T, Chem M (2001) A new model for heavy metal removal in a biosorption column. *Adsorpt Sci Technol* 19:25–43
- Yaneva Z, Marinkovski M, Markovska L, Meshko V, Koumanova B (2008) Dynamic studies of nitrophenols sorption on perflin in a fixed-bed column. *Maced J Chem Chem Eng* 27:123–132

- Yoon YH, Nelson JH (1984) Application of gas adsorption kinetics. I. A theoretical model for respirator cartridge service life. *Am Ind Hyg Assoc J* 45:509–516
- Zhang X, Chen S, Bi HT (2010) Application of wave propagation theory to adsorption breakthrough studies of toluene on activated carbon fiber beds. *Carbon* 48:2317–2326